www.czasopisma.pan.pl PAN www.journals.pan.pl
Opto-Electronics Review 27 (2019) 321–328

Contents lists available at ScienceDirect

Opto-Electronics Review

journal homepage: http://www.journals.elsevier.com/opto-electronics review

Polarization properties of nematic liquid crystal cell with tapered optical fiber

P. Marć*, K. Stasiewicz, J. Korec, L.R. Jaroszewicz, P. Kula

Faculty of Advanced Technologies and Chemistry, Military University of Technology, 2 Gen. S. Kaliskiego St., 00-908, Warsaw, Poland

ARTICLE INFO

Article history:
Received 23 June 2019
Received in revised form 9 October 2019
Accepted 15 October 2019
Available online 14 November 2019

Keywords:
Liquid crystals
Optical fibers
Polarization
Polar decomposition
Singular-value decomposition
Optical losses
Depolarization
Dichroism
Birefringence

ABSTRACT

In the paper, an extended analysis of the polarization properties of a liquid crystal cell with a biconically tapered single-mode telecommunication optical fiber was presented. These properties are a result of a sample geometry and used LC materials. They were analyzed by using two theoretical models based on the matrix decomposition methods, i.e., polar and singular-value one. By measuring Mueller matrices, information about losses, depolarization, dichroism and birefringence was obtained. In the experiment two types of tested samples filled with well-known 6CHBT and E7 liquid crystals were prepared and all optical parameters were shown as the voltage dependence. The tested samples have dichroic properties and for both models calculated PDL is similar and it increases from 2.6 to 6.6 dB for E7 and from 0.4 to 2.7 dB for 6CHBT with voltage changes within the range of 40 – 190 V. Optical losses simultaneously decrease from 30 dB to 27 dB and from 36 dB to 28 dB, respectively. The birefringence properties cannot be directly comparable due to differences between both applied models but voltage fluctuations of these parameters are not significant. These results confirm expected dichroic properties of designed device and complete knowledge about its working principles. Moreover, presented analysis validates usefulness of the singular-value decomposition model applied to dichroic optical fiber elements.

Introduction

Unique optical properties of liquid crystals (LCs) are extensively studied since the late 60-ties of the last century. Their successful industrial applications in the LC displays' technology were associated with the huge efforts of many scientists and have created an enormous space for academic research. The simultaneous development of the optical sensors technologies has enabled the search for hybrid transducers which merge advantages of LCs and optical fibers. In an optical fiber light is strongly confined in its core. Therefore, in order to have an access to the guided light from outside of the fiber, the main problem is to process a fiber material. Tapering of the fiber is an easy and low-cost technology which allows for the partial propagation of light in the material surrounding the original optical fiber as an evanescent wave [1,2]. A few useful glass processing techniques were developed in this scope. The most often used techniques are thermo-mechanical [2,3], chemical [4] or laser [5] treatments of the optical fiber in order to reduce its size in both the cladding and the core [1–3,5] or the cladding removal only [4]. Those processes have led to a design of new types of optical fiber transducers for sensors as a single taper [2–4] or periodical multi-tapers as long-period gratings [5]. Extended feasibility of the tapered optical fibers was reached after a proper functionalization of its tapered part by deposition of additional material layers to increase the sensitivity of the sensors' transducer [6,7] including a surface plasmon resonance effect, as well [8].

The advantages of the combination of a tapered optical fiber and LCs technologies with a discussion of the general light propagation properties were noticed quite early [9–11]. The most recent studies have resulted in a design of the optical elements allowing to observe different optical phenomena. The magneto-optic [12] and thermo-optic [13] effects in the resonant optical structures were observed when light interacts with cylindrical glass capillary filled with ferronematic and nematic LCs, respectively. Light propagated through the tapered optical fiber, and its interaction with spherical LC microdroplets allows to measure thermo-optic properties, as well. Such elements have a prediction for their use as a transducer to a temperature sensor [14].

In mentioned above designs, the standard single-mode optical fibers were used, but development of photonic crystal fibers (PCF) has enhanced research capacities. Tapered PCF coated by LC was used for a design of temperature sensor in interferometric configuration [15]. On the other side, the air-holes' lattice arrangement around the central part of the PCF can be used to modify their propagation properties when air-holes are filled with another material [16]. Filling this type of optical fibers with LCs has resulted in a

* Corresponding author.
E-mail address: pawel.marc@wat.edu.pl (P. Marć).

https://doi.org/10.1016/j.opelre.2019.10.001
1230-3402/

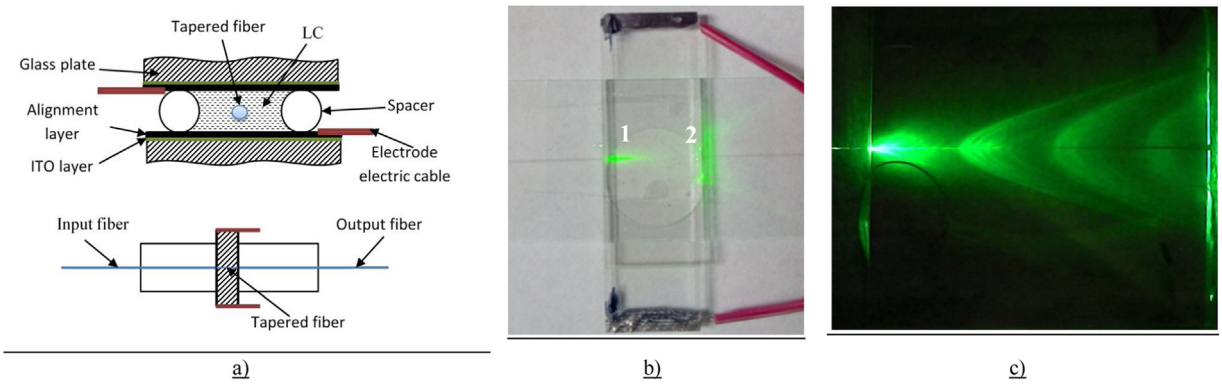

Fig. 1. The scheme - a) and images - b) of the LCC a with tapered optical fiber, and - c) reflections from the top and bottom glass plates of the conical sheets of the radiation modes inside the LCC.

new class of optical fibers named Photonic Liquid Crystal Fibers (PLCF) [17]. The extensive studies of such structures directed for sensor applications [11,18–20] need investigation of their polarization properties regarding the optical anisotropy of the used LCs, as well.

So far, our researches have concerned the electro-optic properties of the liquid crystal cells (LCCs) with a tapered optical fiber where the possibility of intensity modulation and spectral characteristics were shown [21–23]. Design of the tested sample consists of a tapered single-mode telecommunication optical fiber integrated with a standard LCC. Authors' experiences in the manufacturing process of optical fiber biconical tapers by the Fiber Optic Taper Element Technology (FOTET) system [2] and LCCs' assembling have allowed for making the measuring samples. In the research were used two nematic LCs named E7 and 6CHBT. Both materials are described in the literature and often used in tests [24–27]. Their main difference is the size of molecules. E7 is a mixture of four compounds with a relatively small molecule, while 5CHBT is a single NLC component with relatively large molecules. Moreover, ordinary and extraordinary refractive indices of E7 are higher than 6CHBT and the influence of this parameter was also analyzed [22]. These materials with similar sample configuration, synthesized at our university, were previously used as a tunable filter in visible range [21,23].

Current studies are related to polarization properties of such optical structure obtained on the base of polarimetric measurement where first tests were shown in Ref. 28. Generation of the selected states of polarization (SOPs), as input Stokes vectors, and measurement of their changes, as output Stokes vectors, allow for calculating Mueller matrix of the tested sample. Successive calculations of Muller matrices for each voltage give full information about losses, depolarization, dichroism, and retardance of the tested optical element [29]. As the first step of theoretical considerations, optical losses and depolarization were calculated. Analysis of the Average Degree of Polarization (AvDOP) parameter showed that tested samples can be considered as non-depolarizing elements [30]. The next step, the classic matrices' decomposition algorithm based on polar decomposition [31] has been used for polarization study. This model allows to analyze dichroic and birefringence properties of measured samples. Based on these data it is possible to calculate such parameters as: linear and circular dichroisms, linear retardance, optical rotation, and orientation angle [30]. Due to the fact that polar decomposition model is not symmetric, cascade connection of diattenuator, elliptic retarder and depolarizer were used as the first approximation. However, taking into account the symmetry of the sample (input and output optical fibers and the LCC with a tapered fiber between them) a singular-value decomposition model [32] for polarization investigation has been used, as well. In this model the optical fibers are described as the linear retarders whereas the LCC with the tapered fiber is described as a dichroic element defined by a combination of linear diattenuator and horizontal retarder.

Technology and principles of work of a nematic liquid crystal cell with tapered optical fiber

The FOTET system was used to tapering an optical fiber SMF28e - by heat and pull technique in which a low-pressure flame softens glass of fiber and allows for a reduction of its external diameter in the form of a biconical tapper structure [2]. Next, the tapered fiber is integrated with the LCC structure according to the sample design previously presented in Ref. 18 with the scheme shown in Fig. 1a). The main parameters of the manufactured adiabatic taper are as follows: 20.0 mm waist length, around 12.0 μm waist diameter, optical taper losses of about 0.2 dB@1550 nm. The tested LCCs are 40 μm thick with a rubbing direction of alignment layers perpendicular to the tapered optical fiber and they were filled with 6CHBT or E7 LCs' mixtures. Thickness and rubbing direction were optimal for devices [22]. The selected LCs were chosen due to the fact that they are well known materials with different extraordinary refractive indices of 1.672 for 6CHBT and 1.739 for E7 [22]. This gives possibility to check the influence of used LC on polarization parameters of the analyzed device. The image of LCCs with the tapered optical fiber is shown in Fig. 1b). The principles of work of this type of optical fiber device was previously presented in Refs. [9] and [10]. There were described basic electro-optic properties of LCC with a tapered optical fiber. Polarization properties of these devices were only mentioned in Ref. 9. In order to measure thermo-optic properties of such optical device, the selected LC was mixed with water to reduce a refractive index of the mixture to be less than silica [10]. In presented study, the selected LCs have both ordinary and extraordinary refractive indices higher than silica [22]. In such boundary conditions the tapered fiber cladded by these LCs does not transmit the light. However, waveguiding properties of this optical element are a result of the geometry of the LCC, as is shown in Fig. 1b).

In Fig. 1b) two illuminated from inside of the sample areas can be distinguished in places where light enters (1) and exits the sample (2). First of them, marked (1) shows radiation modes excited in the glued connection between the optical fiber and glass plates and second area, whereas marked (2) shows refracted light at the edges of glass plates. These modes are excited in this structure due to the fact that refractive index of LC is higher than the silica of the optical fiber. Energy of radiation modes in the plane of the sample is lost due to diffraction what is visible as enlarged illuminated area (2) at the right edge of the sample [Fig. 1b)]. However, in a

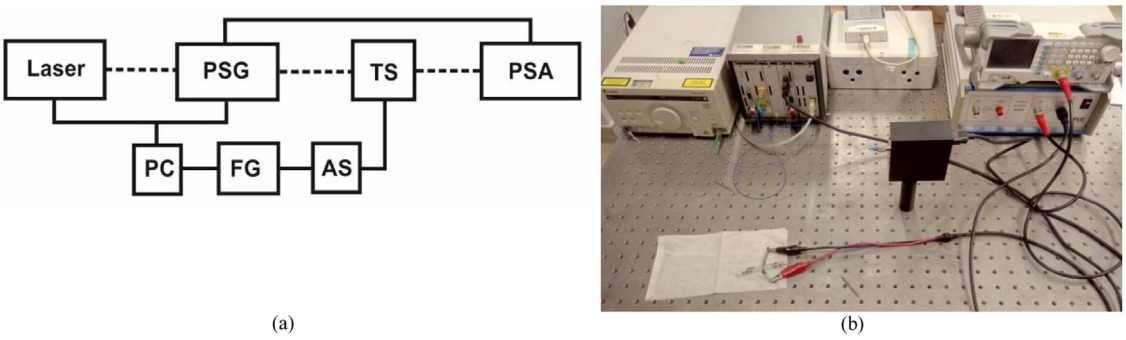

Fig. 2. Polarimetric set-up for polarization properties' measurements of the LLC with tapered optical fiber: (a) scheme, (b) image.

plane perpendicular to the sample these modes reflect from glass plates [see illuminating areas in Fig. 1c)] and their fraction couple back to the optical fiber when the light exits the sample. The amount of measured intensity depends on input SOP, as well as an applied voltage which reorients and aligns LCs' director. These dichroic properties of device make a unique opportunity to analyze polarization properties by using different theoretical models.

Experimental measurements and data analysis

Polarization properties of designed samples were measured by using a polarimetric configuration set-up, as is shown in Fig. 2. It consists of a laser light source (Laser), polarization state generator (PSG), tested sample (TS) and polarization state analyzer (PSA). TS was driven by the amplified signal (AS) from the function generator (FG). PSG, PSA, and TS were controlled by a personal computer (PC), and all data were acquired and analyzed by dedicated software implemented in PC [27]. It is worth to mention that there are also other optical fiber based measurement methods of polarization parameters [33].

As a light source was used a high power laser TSL-210 V (Santec, Japan) working at 1550 nm with the optical power of 20 mW. Deterministic polarization controller DPC 5500 (Thorlabs, Sweden) and polarimeter PAX5710 (Thorlabs, Sweden) were used as PSG and PSA, respectively. To characterize electro-optic properties of TS, function generator DG1022 (RIGOL, China) and voltage amplifier A400D (FLC Electronics, Sweden) have been used as FG and AS, respectively. They allow to generate the square waveforms with a constant frequency of 1 kHz and amplitudes within the range of 0–200 V.

The determination of the Mueller matrix was used in the investigation of polarization properties of the analyzed devices. Selected set of input SOPs generated by PSG was defined as input Stokes vectors S^i_{PSG}. SOP changes after passing through the TS were measured by PSA as output Stokes vectors S^i_{PSA}. Next, the Mueller 4×4 matrix (M_{ex}) at each of applied voltage was calculated based on relation [34]:

$$S^i_{PSA} = M_{ex}\, S^i_{PSG}. \tag{1}$$

Specific input SOPs' generation was necessary to simplify the calculation of the M_{ex} elements. As the sets of input Stokes vectors S^i_{PSG} were used: four linear SOPs as horizontal, vertical, with azimuth +45 deg and with azimuth −45 deg, and a pair of circular one, i.e., right and left. For each of the mentioned above input SOPs' respective output Stokes vector were measured and, next, all elements of the Mueller matrix were calculated [34].

In general, the Mueller matrix carries information about losses, depolarization, dichroism, and birefringence [29–32,34–36]. Losses are treated as an isotropic optical attenuation, and they are defined by a single value. Depolarization process can be treated as isotropic or anisotropic and is represented by a single value or at least three coefficients obtained from Mueller matrix elements, respectively [30]. Dichroism, also named diattenuation, shows anisotropy of optical losses whereas the birefringence transforms input SOP and can be defined by linear and circular birefringence [29,31]. Dichroism and birefringence are three element vectors calculated from the Mueller matrix. Therefore, from total 16 elements of any Mueller matrix only, at least ten elements are independent.

In Fig. 3 plots of sixteen raw Mueller matrices M elements (m_{ij}) calculated for TSs with 6CHBT and E7 LCs were shown. To emphasize their electro-optic properties, each matrix element was normalized to m_{ex00} element. Presented plots show changes of appropriate matrix elements while the driven voltage amplitude was changed from 40 V up to 190 V.

Uncertainty analysis is complex in case of experimental Mueller matrix because each element of this matrix depends on six measured variables. Application of the combined standard uncertainty allows to build uncertainty matrix. Analysis of matrices obtained from measurements data showed that their maximal value does not exceed 2%. Moreover, equally important is the filtering procedure which reduces measurement noise and finite accuracy of the used set-up by transformation of the experimental matrices to physically realizable semi-definite Hermitian one [29–32,34–37].

As the first step, the optical losses (L) and AvDOP were calculated from the filtered experimental matrices M_f by using the following relations [30]:

$$\mathrm{L} = -10log_{10}\left[m_{f\,00}\right],\ AvDOP = \frac{1}{4\pi}\int_0^{\pi}\int_{-\frac{\pi}{4}}^{\frac{\pi}{4}} DOP(\phi,\varepsilon)\cos 2\varepsilon d\phi\, d\varepsilon \tag{2a}$$

$$DOP(\phi,\varepsilon) = \frac{\sqrt{S_1^{'2}(\phi,\varepsilon)+S_2^{'2}(\phi,\varepsilon)+S_3^{'2}(\phi,\varepsilon)}}{S_0^{'}(\phi,\varepsilon)} if S^{'} = M_f\, S\ and = S = \begin{bmatrix} 1 \\ \cos\phi\cos\varepsilon \\ \sin\phi\cos\varepsilon \\ \sin\varepsilon \end{bmatrix}, \tag{2b}$$

where: m_{f00} is the element of filtered Mueller matrix, φ and ε are the azimuth and ellipticity of input SOP represented by Stokes vector S.

The plots of mentioned above two optical parameters for investigated TSs are shown in Fig. 4. Losses [Fig. 4(a)] for both LC materials are high and decrease as the voltage increases. The dynamic range of these changes is of about 7.6 dB for E7 and about 2.5 dB for 6CHBT. The main source of losses are diffraction in-plane of LCC and infrared absorption of the LCs. However, their voltage

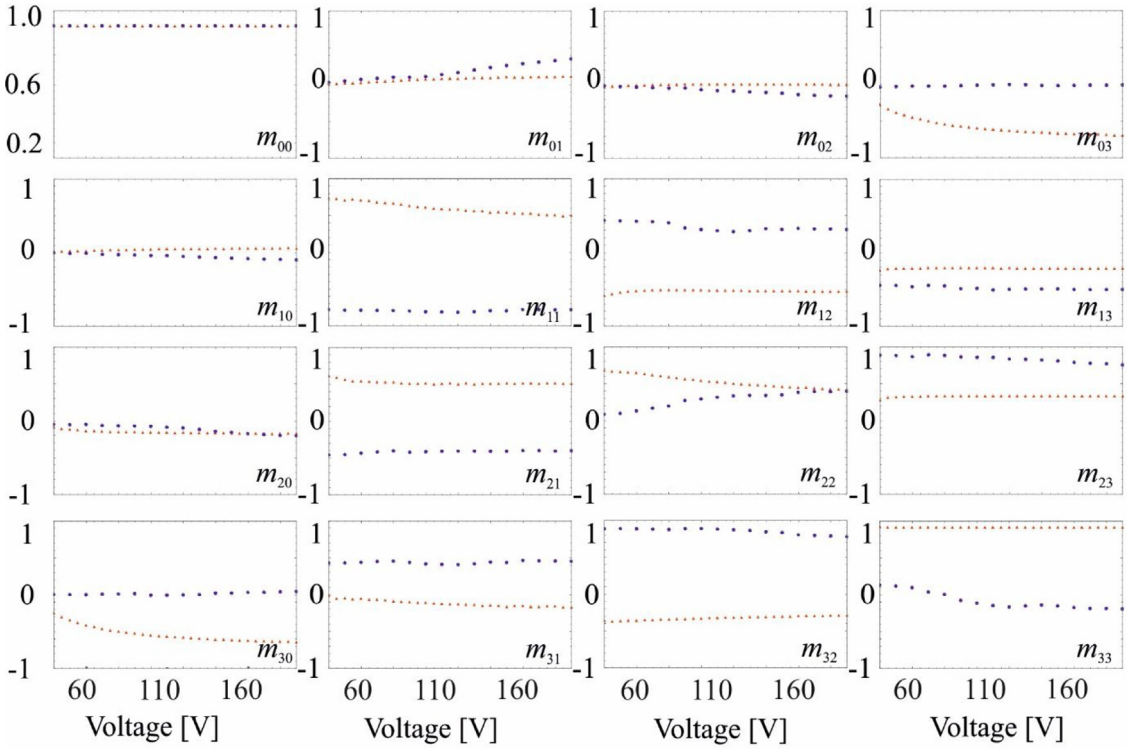

Fig. 3. The calculated normalized elements of Mueller matrices of TSs with 6CHBT (blue dots) and E7 (red triangles) LCs *vs.* voltage.

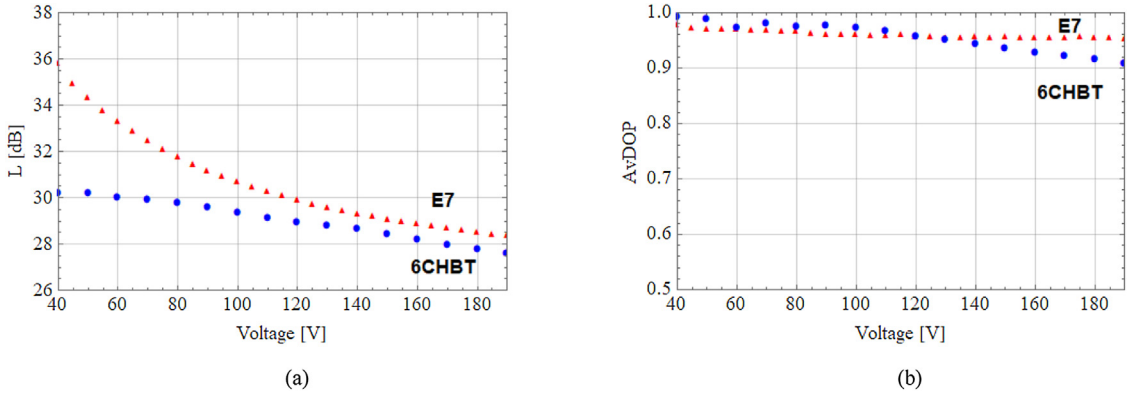

Fig. 4. Losses (L) - (a) and Average Degree of Polarization (AvDOP) – (b) *vs.* voltage for TSs.

dependence can be connected with reordering of LC molecules by electrical field in designed LCC. The molecular arrangements of the LC close to both glass plates [Fig. 1a)] are uniform due to applied alignment layers and director is in-plane with the glass plates of the LCC and perpendicular to the tapered fiber. In the center of the LCC, the molecular arrangement has more statistical distribution. With increase of the voltage director rotates to be perpendicular to glass plates and this results in an increase of refractive index of the LC from ordinary to extraordinary one. For this reason, more optical power is coupled back to the tapered fiber at the end of the sample.

AvDOP [Fig. 4(b)] of the tested samples are close to unity for both materials and, therefore, depolarization properties can be regarded as negligible. Such a result confirms elimination of this effect from calculations and sufficiently simplifies further analyses.

Applying the commonly used polar decomposition (PD) method to the filtered and normalized Mueller matrix M^1 allows to show TS as a concatenation of two matrices: retarder M_R – includes information about birefringence and diattenuator, M_D – informs us about dichroic properties of the sample. Mathematically, this can be written as follows [28,29,34]:

$$M^1 = \begin{bmatrix} 1 & \vec{D}^T \\ \vec{P} & m^1 \end{bmatrix} = M_R \cdot M_D = \begin{bmatrix} 1 & \to 0^T \\ \vec{0} & m_R \end{bmatrix} \cdot \begin{bmatrix} 1 & \vec{D}^T \\ \vec{D} & m_D \end{bmatrix}, \tag{3}$$

where: $\vec{P}^T = \left[m^1_{10}, m^1_{20}, m^1_{30}\right]$ and $\vec{D}^T = \left[m^1_{01}, m^1_{02}, m^1_{03}\right]$ are parts of the first column (polarizance vector) and the first row (diattenuation vector) of the analyzer matrix M^1, respectively. Additionally, m^1 is 3×3 submatrix of matrix M^1, whereas $\vec{0}^T = [0, 0, 0]$ is a null row vector.

Existing in (3) submatrices m_R and m_D are 3×3 matrices calculated as:

$$m_D = a\, I_3 + b\, \left(\vec{D}\,\vec{D}^T\right), \quad m_R = \frac{1}{a}\left[m^1 + b\, \left(\vec{P}\,\vec{D}^T\right)\right] \tag{4}$$

where: $a = \sqrt{1 - \left|\vec{D}\right|^2}$, $b = 1 - a$, I_3 – 3×3 identity matrix.

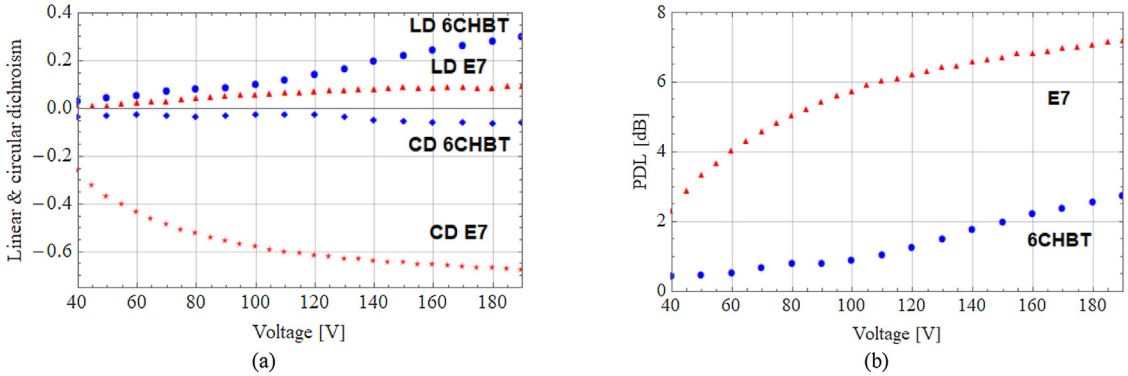

Fig. 5. Dichroic property of tested samples: (a) linear (LD) and circular (CD) dichroism and (b) PDL.

Dichroic properties of the measured TS can be analyzed directly from diattenuation vector $\vec{D}$. It is defined by three elements where the first two describe its linear dichroism (LD) which is related to a linear polarizer property while the third one describes circular dichroism (CD), i.e., circular polarizer property. They are defined as follows [29]:

$$\mathrm{LD} = \sqrt{(m_{01}^1)^2 + (m_{02}^1)^2};\ \mathrm{CD} = m_{03}^1. \tag{5}$$

In optical fiber technology, a cumulative parameter used to define a dichroic property of the optical fiber is polarization dependent loss (PDL) and it can be calculated by the following definition [34]:

$$\mathrm{PDL} = 10log_{10}\left[\frac{1+|\vec{D}|}{1-|\vec{D}|}\right]. \tag{6}.$$

Application of relations (4–6) allows for the plot of linear and circular dichroism, as well as PDL characteristics for both tested TSs as is presented in Fig. 5.

As one can see, the sample with 6CHBT LC shows linear dichroism (LD 6CHBT) while the sample with E7 demonstrates circular dichroism (CD E7). Such difference, in the author's opinion, is a result of used model and cannot be connected to the geometry of designed TS or differences in optical properties of the used LCs. Additionally, in both samples, dichroic property grows with voltage which is associated with Fresnel's' reflection on the interface of LCs and glass plates.

Taking into account the above discrepancy of the dichroic property of both TSs, it is more convenient to analyze cumulative information about diattenuation displayed as PDL characteristics as is shown in Fig. 5(b). Comparing dynamic ranges of this parameter, PDL grows from 0.4 dB to 2.8 dB for 6CHBT and from 2.3 dB to 6.6 dB for E7. This fact suggests that the application of the last LC with higher extraordinary refractive index stronger influences the polarizing property of the tested optical element. Additionally, it can be observed that the PDL changes for both samples correlate with losses plotted in Fig. 4(a). For both LCs correlation coefficients are close to −1.

The birefringence property in the presented PD model is simulated by two optical elements, i.e., circular and linear retarders are characterized by optical rotation ψ and linear retardance (phase shift) δ, respectively. Linear retarder has an orientation angle α with regard to the horizontal axis [35]. Taking into account relations (3) and (4) above three parameters are defined as follows [31,35]:

$$\psi = \frac{1}{2}arctan\left[\frac{A}{B}\right];\ \delta = arccos\left[\sqrt{A^2+B^2}-1\right] \tag{7a}$$

$$\alpha = \frac{1}{2}arctan\left[\frac{\alpha_2}{\alpha_1}\right] \tag{7b}$$

where: $A = m_{R21} - m_{R12}$; $B = m_{R11} + m_{R22}$; m_{Rjk} – suitable elements of submatrices m_R, whereas $\alpha_i = \frac{1}{Sin\,\delta}\sum_{j,k=1}^{3}\varepsilon_{ijk}m_{Rjk}$; ε_{ijk} - Levi-Cavity tensor, $i, j, k = 1, 2, 3$.

Fig. 6 presents changes in birefringence parameters for the investigated TSs as a function of the applied voltage. They are represented by optical rotation [Fig. 6(a)] and linear retardance or phase shift [Fig. 6(b). Both parameters grow with voltage and optical rotation changes of about 0.1 rad while changes of phase shifts are stronger for 6CHBT and reach 0.4 and it is almost constant for E7. The orientation angle α remains unchanged in the full range of applied voltage for both investigated TSs, as is shown in Fig. 6(c). So, the dynamic ranges of these changes are weaker than their dichroic parameters but still obvious. Additionally, high correlation of the phase shifts δ and PDLs of both used LCs [Fig. 5(b)] is observed.

As was mentioned above, it is difficult to find a proper explanation of the discrepancy shown in Fig. 5(a) between linear and circular dichroic properties of tested samples. However, taking into account the geometry of TSs, another theoretical model was proposed in further analysis. It is related to the singular-value decomposition (SVD) method [32]. The most important advantage of this model is its symmetry because the tested optical element is considered as a concatenation of three components, i.e., two linear retarders with a partial polarizer with retardance between them. The LCC with the tapered optical fiber fits this model because it consists of an input and output optical fibers and dichroic LCC with tapered optical fiber. Therefore, input and output fibers in a proper experiment preparation can be treated as linear retarders whereas the LCC can be the partial polarizer.

In the proposed SVD method normalized and filtered Mueller matrix M^1 can be mathematically represented as follows [31]:

$$M^1 = M_U[\alpha_2, \delta_2]\,M_{RD}[T, t, \gamma\,]\,M_V^T[\alpha_1, \delta_1], \tag{8}$$

where: M_U and M_V are the matrices of retarders with linear retardances δ_i and orientation angles α_i, M_{RD} is the matrix of a partial polarizer with respective relative maximum T and minimum t transmissions and retardance γ.

In the first step of calculations, with the help of a Householder transformation, matrices M_U and M_V were calculated by using the following formulas [32]:

$$M_U = M_{H1}D\,and\,M_V = M_{H2}D \tag{9}$$

where:

$$M_{Hi} = \begin{bmatrix} 1 & \vec{0}^T \\ \vec{0} & H_i \end{bmatrix},\ H_i = I_3 - \frac{2\,\vec{h}_i^{\,T}\cdot\vec{h}_i}{|\vec{h}_i|}$$

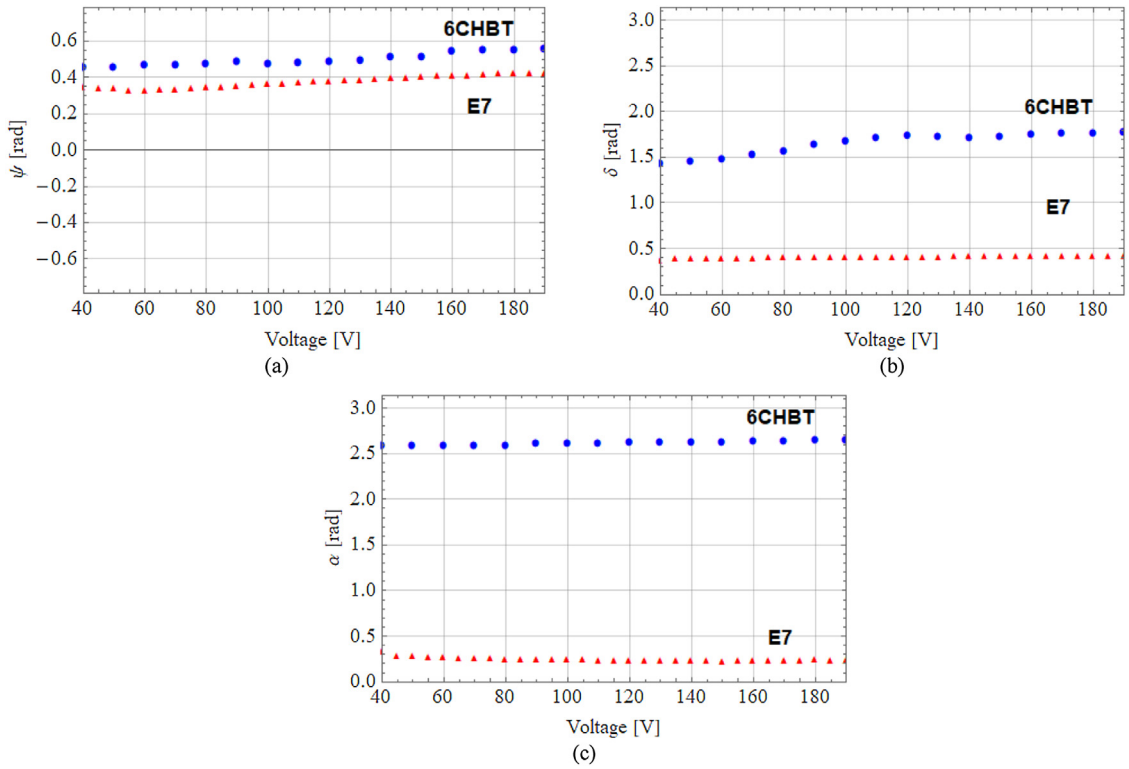

Fig. 6. Calculated birefringence properties of TSs: (a) optical rotation ψ, (b) linear retardance δ, and (c) orientation angle α as a function of the applied voltage.

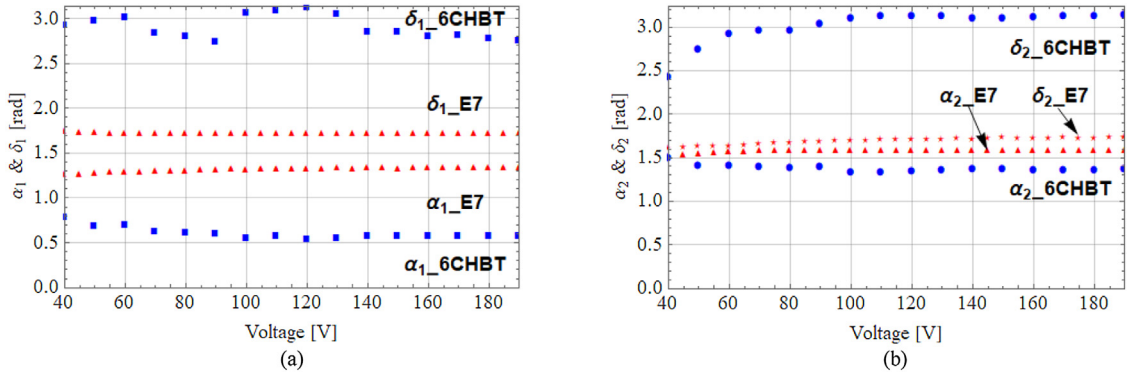

Fig. 7. Linear retarders properties of the input - (a) and output - (b) optical fibers of the tested samples with 6CHBT and E7 LCs.

$$\vec{h}_i = \begin{cases} \vec{P}^T - \left[\varepsilon\left|\vec{P}\right|, 0, 0\right]; i = 1 \\ \vec{D}^T - \left[\varepsilon\left|\vec{d}\right|, 0, 0\right]; i = 2 \end{cases}, \; D = \begin{bmatrix} 1 & 0 & 0 & 0 \\ 0 & 1 & 0 & 0 \\ 0 & 0 & 1 & 0 \\ 0 & 0 & 0 & -1 \end{bmatrix}$$

and ε=±1 – defines horizontal (+) or vertical (-) orientation of maximum transmission axis of the partial polarizer.

Matrices M_U and M_V are described by two pairs of parameters, i.e., (α_1, δ_1) and (α_2, δ_2) which are calculated by using respective formulas from relations (7).

Next step is the calculation of the so-called *M'* matrix, which has a 2 × 2 block-diagonal form [32]:

$$M' = M_U^T M M_V \tag{10a}$$

and

$$M' = \begin{bmatrix} \frac{1}{2}(T+t) & \frac{1}{2}\varepsilon(T-t) & 0 & 0 \\ \frac{1}{2}\varepsilon(T-t) & \frac{1}{2}(T+t) & 0 & 0 \\ 0 & 0 & \sqrt{Tt}\cos\gamma & \sqrt{Tt}\sin\gamma \\ 0 & 0 & -\sqrt{Tt}\sin\gamma & \sqrt{Tt}\cos\gamma \end{bmatrix}. \tag{10b}$$

The above matrix represents a linear partial polarizer with horizontal or vertical orientation (left top corner 2 × 2 block) and linear retarder defined by angle γ (right bottom corner 2 × 2 block). Parameters *T*, *t*, γ are easy to be calculated by using elements with both blocks. Additionally, the cumulative value of PDL can be calculated with the standard formula [34]:

$$\mathrm{PDL} = 10 log_{10}[\frac{T}{t}]. \tag{11}$$

Taking into account the TS geometry and the fixed horizontal polarizer used in PSA, the value of ε equals -1.

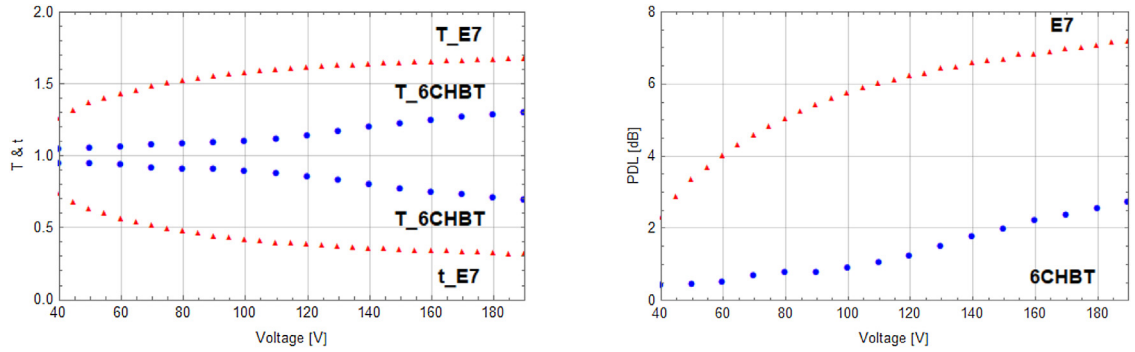

Fig. 8. Relative maximum T and minimum t transmissions – (a) and PDL characteristics – (b) of the vertically oriented linear partial polarizer with 6 CHBT and E7 LCs.

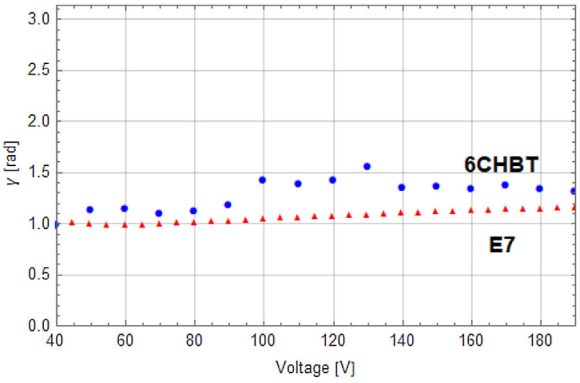

Fig. 9. The retardance of the vertically oriented linear polarizer with 6CHBT and E7 LCs.

In Figs. 7–9 the polarization parameters of input and output retarders and linear partial polarizer with retardance are presented.

Voltage dependence of optical parameters for input linear retarders (Fig. 7) of the sample based on E7 LC is very weak and does not exceed 0.1 and for output retarder changes are less than 0.2. For 6CHBT LC material fluctuations of orientations angles of both retarders are between 0.2 – 0.3. Changes of linear retardance of these elements are stronger and are of around 0.4 for δ_1 and of 0.7 for δ_2.

Calculated partial polarizer properties represented as relative transmissions T and t were shown in Fig. 8(a) and their cumulative PDL characteristics are plotted in Fig. 8(b).

Relative extremes T and t of both materials are symmetrical around the value of one [Fig. 8(a)]. Their differences grow with voltage showing increase of polarizing properties. Their cumulative PDL characteristics [Fig. 8(b)] are in a very good agreement with data calculated for the PD model as is shown in Fig. 5(b). The last parameter of this model – retardance γ of the partial polarizer is shown in Fig. 9.

Retardance for E7 LC based sample has small changes less than 0.18 within the range of the applied voltage while for the sample with 6CHBT material has stronger fluctuations with maximal deference equal to 0.6.

Conclusions

In the paper extended studies of the LCC with tapered single-mode telecommunication optical fiber are presented. Calculated measurements of optical parameters based on Mueller matrix show that this type of a hybrid optical fiber device has high losses and dichroic properties. Both of them result mostly in the geometry of the sample. Birefringence properties are rather weak, as well as its depolarization properties which are even negligible. Application of two different LC materials shows that using E7 material with higher refractive index allows to improve its dichroic properties to have dynamic range twice better than for 6CHBT. Moreover, electro-optic dependence of birefringence in the sample with E7 has less fluctuation than the other one. Unique dichroic properties of the manufactured samples give possibility to validate singular-value decomposition model which is dedicated to analysis optical systems consisting of partial polarizers placed between linear retarders. In Authors' best knowledge this model was used for the first time to characterize optical fiber element. Moreover, calculated PDL proved usefulness of both applied models to describe optical properties of such hybrid optical devices.

Author contributions

P.M. concept of the polarization properties measurement and theoretical analysis, K. A. S. and J.K. technology of tapered optical fiber, designing and manufacturing of the tested LCCs, L.R.J. analysis and interpretation of the measurement data, P.K. synthesis of liquid crystals, P.M. and L.R.J. writing draft, review and editing.

Funding

This work was supported by the Ministry of National Defence by research grants: GBMON/13-995/2018/WAT and Ministry of Higher Education as a statutory activity project PBS -23 - 898.

Declaration of Competing Interest

The authors declare no conflict of interest.

Acknowledgements

This work was supported by the Ministry of Science and Higher Education as a statutory activity PBS – 898 and the Ministry of National Defense Republic of Poland project no. GBMON/13-995/2018/WAT. The authors would like to thank, prof. Wiktor Piecek and Przemysław Morawiak from Division of Physics and Technology of Crystals, MUT for their technological support in a liquid crystal cells design.

References

[1] T.A. Birks, Y.W. Li, The shape of fiber tapers, J. Lightwave Technol. 10 (1992) 432–438, http://dx.doi.org/10.1109/50.134196.
[2] K.A. Stasiewicz, R. Krajewski, L.R. Jaroszewicz, M. Kujawińska, R. Świłło, Influence of tapering process on changes of optical fiber refractive index

distribution along with a structure, Opto-Electron. Rev. 18 (2010) 102–109, http://dx.doi.org/10.2478/s11772-009-0030-y.
[3] J. Love, W.M. Henry, W.J. Stewart, R.J. Black, S. Lacroix, F. Gonthier, Tapered single-mode fibers and devices, part 1: adiabaticity criteria, IEE Proc. J. - Optoelectron. 138 (1991) 343–354, http://dx.doi.org/10.1049/ip-j.1991.0060.
[4] Y. Yuan, L. Wang, L. Ding, C. Wu, Theory, experiment, and application of optical fiber etching, Appl. Opt. 51 (2012) 5845–5849, http://dx.doi.org/10.1364/AO.51.005845.
[5] Y. Wang, Review of long-period fiber gratings written by CO2 laser, J. Appl. Phys. 108 (2010) 081101, http://dx.doi.org/10.1063/1.3493111.
[6] K.Q. Kieu, M. Mansuripur, Biconical fiber taper sensors, IEEE Photon. Technol. Lett. 18 (2006) 2239–2241, http://dx.doi.org/10.1109/LPT.2006.884742.
[7] H. Latifi, M.I. Zibaii, S.M. Hosseini, P. Jorge, Nonadiabatic tapered optical fiber for biosensor applications, Photonic Sens. 2 (2012) 340–356, http://dx.doi.org/10.1007/s13320-012-0086-z.
[8] B.D. Gupta, R.K. Verma, Surface plasmon resonance-based fiber optic sensors: principle, probe designs, and some applications, J. Sens. 2009 (2009) 979761, http://dx.doi.org/10.1155/2009/979761.
[9] C. Veilleux, J. Lappiere, J. Bures, Liquid-crystal-clad tapered fibers, Opt. Lett. 11 (1986) 733–735, http://dx.doi.org/10.1364/OL.11.000733.
[10] C. Veilleux, R.J. Black, J. Lappiere, L.W. Reeves, Nematic liquid crystal clad tapered optical fiber with temperature sensing properties, J. App. Phys. 67 (1990) 6648–6653, http://dx.doi.org/10.1063/1.345098.
[11] T.-J. Chen, S.-H. Chen, Propagation of lower-order modes in a radially anisotropic cylindrical waveguide with liquid crystal cladding, J. Lightwave. Technol. 13 (1995) 1698–1705, http://dx.doi.org/10.1109/50.405312.
[12] A. Mahmood, V. Kavungal, S.S. Ahmed, P. Kopcansky, V. Zavisova, G. Farrell, Y. Semenova, Magnetic field sensing using whispering gallery modes in a cylindrical microresonator infiltrated with ferronematic liquid crystal, Opt. Express 25 (2017) 12195–12202, http://dx.doi.org/10.1364/OE.25.012195/.
[13] V. Kavungal, G. Farrell, Q. Wu, A.K. Mallik, Y. Semenova, Thermo-optic tuning of a packaged whispering gallery mode resonator filled with nematic liquid crystal, Opt. Express 26 (2018) 8431–8442, http://dx.doi.org/10.1364/OE.26.008431.
[14] Y. Wang, H. Li, L. Zhao, Y. Liu, S. Liu, J. Yang, Tapered optical fiber waveguide coupling to whispering gallery modes of liquid crystal microdroplet for thermal sensing application, Opt. Express 25 (2017) 918–926, http://dx.doi.org/10.1364/OE.25.000918.
[15] G. Rajan, S. Mathews, G. Farrell, Y. Semenova, A liquid crystal coated tapered photonic crystal fiber interferometer, J. Opt. 13 (2011) 015403, http://dx.doi.org/10.1088/2040-8978/13/1/015403.
[16] P. Marć, N. Przybysz, A. Molska, L.R. Jaroszewicz, Photonic crystal fiber transducers for an optical fiber multilevel temperature threshold sensor, J. Lightwave Technol. 36 (4) (2018) 898–903.
[17] T.R. Woliński, S. Ertman, P. Lesiak, A.W. Domański, A. Czapla, R. Dąbrowski, E. Nowinowski-Kruszelnicki, J. Wójcik, Photonic liquid crystal fibers – a new challenge for fiber optics and liquid crystals photonics, Opto-Electron. Rev. 14 (2006) 329–334, http://dx.doi.org/10.2478/s11772-006-0045-6.
[18] T.R. Woliński, S. Ertman, A. Czapla, P. Lesiak, K. Nowecka, A. Domański, E. Nowinowski-Kruszelnicki, R. Dąbrowski, J. Wójcik, Polarization effects in photonic liquid crystal fibers, Meas. Sci. Technol. 18 (2007) 3061–3069, http://dx.doi.org/10.1364/OFS.2006.ThE58.
[19] S. Ertman, K. Rutkowska, T.R. Wolinski, Recent progress in liquid-crystal optical fibers and their applications in photonics, J. Lightwave Technol. 37 (2019) 2516–2526, http://dx.doi.org/10.1109/JLT.2018.2869916.
[20] J.F. Algorri, D.C. Zografopoulos, A. Tapetado, D. Poudereux, J.M. Sánchez-Pena, Infiltrated photonic crystal fibers for sensing applications, Sensors 18 (2018) 4263, http://dx.doi.org/10.3390/s18124263.
[21] J.E. Moś, M. Florek, R. Wonko, K.A. Stasiewicz, L.R. Jaroszewicz, Influence temperature and electric field on propagation properties of a nematic liquid crystals fiber device, Proc. SPIE 10325 (2017) 103250F, http://dx.doi.org/10.1117/12.2271042.
[22] J. Korec, K.A. Stasiewicz, O. Strzeżysz, P. Kula, J. Moś, L.R. Jaroszewicz, Tapered fibre liquid crystal optical device, Proc. SPIE 10681 (2018) 106810G, http://dx.doi.org/10.1117/12.2271042.
[23] J.E. Moś, M. Florek, K. Garbat, K.A. Stasiewicz, N. Bennis, L.R. Jaroszewicz, In-line tunable nematic liquid crystal fiber optic device, J. Lightwave Technol. 36 (2018) 891–897, http://dx.doi.org/10.1109/JLT.2017.2771368.
[24] H. Tajalli, A. Ghanadzadeh, H. Khoshsima, P. Zhalefar, Electro-optical Kerr effect of nematic mixtures comprised of 6CHBT and 6BOBT, Opto-Electron. Rev. 16 (2008) 386–389, http://dx.doi.org/10.2478/s11772-008-0037-9.
[25] N. Tomasovicova, P. Koacansky, M. Koneracka, The structural transitions in 6CHBT- based ferronematic droplets, J. Phys-Condens. Mat. 20 (2008), 204123, http://dx.doi.org/10.1088/0953-8984/20/20/204123.
[26] L. Bedjaoui, N. Gogibus, B. Ewen, T. Pakula, X. Coqueret, M. Benmouna, U. Maschke, Preferential solvation of the eutectic mixture of liquid crystals E7 in a polysiloxane, Polymer 45 (2004) 6555–6560, http://dx.doi.org/10.1016/j.polymer.2004.07.050.
[27] R. Dąbrowski, J. Dziaduszek, T. Szczuciński, 4-(trans4′alkylcyclohexyl)isothio-cyanatobenzenes a new class of low-melting stable nematics, Mol. Cryst. Liq. Cryst. 102 (1984) 155–160, http://dx.doi.org/10.1080/01406568408072065.
[28] P. Marć, K.A. Stasiewicz, J. Korec, M. Kwiatkowska, O. Strzeżysz, P. Kula, L.R. Jaroszewicz, Polarization properties of an optical fiber biconical taper with a liquid crystal cladding, Proc. SPIE 11045 (2019) 110450D, http://dx.doi.org/10.1117/12.2520889.
[29] D. Goldstein, Polarized Light, second ed., Marcel Dekker Inc., New York & Basel, 2003.
[30] J. Boulvert, G. Le Brun, B. Le Jeune, J. Cariou, L. Martin, Decomposition algorithm of an experimental Mueller matrix, Opt. Commun. 182 (2009) 692–704, http://dx.doi.org/10.1016/j.optcom.2008.10.076.
[31] S. Lu, R.A. Chipman, Interpretation of Mueller matrices based on polar decomposition, J. Opt. Soc. Am. A 13 (1996) 1106–1113, http://dx.doi.org/10.1364/JOSAA.13.001106.
[32] R. Ossikovski, Interpretation of nondepolarizing Mueller matrices based on singular-value decomposition, J. Opt. Soc. Am. A 25 (2008) 473–482, http://dx.doi.org/10.1364/JOSAA.25.000473.
[33] L.R. Jaroszewicz, P. Marć, In-line fiber-optic polarization analyzers for sensor application, IEEE Sens. J. 3 (2003) 71–79, http://dx.doi.org/10.1109/JSDEN.2003.809022.
[34] E. Collett, Polarized Light in Optical Fiber, The PolaWave Group, Lincroft New Jersey, 2003.
[35] N. Gosh, M.F.G. Wood, I.A. Vitkin, Mueller matrix decomposition for extraction of individual polarization parameters from complex turbid media exhibiting multiple scattering, optical activity, and birefringence, J. Bio. Opt. 13 (2008), http://dx.doi.org/10.1117/1.2960934, 044036-1 14.
[36] P. Kula, N. Bennis, P. Marć, P. Harmata, K. Gacioch, P. Morawiak, L.R. Jaroszewicz, Perdeuterated liquid crystals for near infrared applications, Opt. Mat. 60 (2016) 209–213, http://dx.doi.org/10.1016/j.optmat.2016.06.047.
[37] J.J. Gil, On optimal filtering of measured Mueller matrices, App. Opt. 55 (2016) 5449–5455, http://dx.doi.org/10.1364/AO.55.005449.